Development of Free Vortex Wake Model for Wind Turbine Aerodynamics under Yaw Condition

Hamidreza Abedi*
Chalmers University of Technology, 412 96, Gothenburg, Sweden
Lars Davidson,†
Chalmers University of Technology, 412 96, Gothenburg, Sweden
Spyros Voutsinas, ‡
National Technical University of Athens, Athens, Greece

The aerodynamics of a wind turbine is governed by the flow around the rotor. One of the most severe operating conditions for a wind turbine is the yaw misalignment, when the mean upstream flow is not perpendicular to the rotor plane. This asymmetrical flow changes significantly the velocity field around the rotor blades which in turn reduces power production of the wind turbine. It also makes a periodic load variation along the rotor blade which accordingly increases the fatigue load from the design point of view. In this paper, the effect of the skewed wake, due to the yaw misalignment, on the wake aerodynamics of wind turbine is studied. For this purpose, an in-house Vortex Lattice Free Wake (VLFW) code, based on the potential, inviscid and irrotational flow, is developed. The results are compared with the MEXICO wind tunnel measurements. For the axial traverses, there is a good agreement between the measured axial (w) and tangential (u) velocity components and the simulations. Although the magnitude of the mean radial velocity component (v) is fairly well predicted, its fluctuation is not captured by the simulation. Moreover, for the radial traverses, the simulations are remarkably verified by the measurements.

Nomenclature

Γ	Circulation, m^2/s
$\vec{V}$	Velocity vector, m/s
Ω	Rotational velocity, rad/s
$\vec{r}$	Position vector, m
γ	Vorticity distribution per length, m/s
t	time, s
$\vec{V}_\infty$	free stream velocity vector, m/s
u	Velocity component in the x direction, m/s
v	Velocity component in the y direction, m/s
w	Velocity component in the z direction, m/s
Subscript	
i, j	Panel index
$T.E.$	Trailing edge
ind	Induced
rot	Rotational
W	Wake
tot	Total

*Ph.D. Candidate, Division of Fluid Dynamics, Department of Applied Mechanics & Swedish Wind Power Technology Centre (SWPTC)
†Professor, Division of Fluid Dynamics, Department of Applied Mechanics & Swedish Wind Power Technology Centre (SWPTC)
‡Associate Professor, Fluid Section, School of Mechanical Engineering

I. Introduction

The asymmetric flow around the operating wind turbine due to the yawed incoming flow creates an unsteady and 3D aerodynamic environment which has not been well understood yet. This complexity is more pronounced when the aeroelastic response of rotor blades is taken into account.

There are different methods to describe the rotor aerodynamics of a wind turbine depending on levels of complexity and accuracy, such as the Blade Element Momentum (BEM) theory and solving the Navier-Stokes equations using Computational Fluid Dynamics (CFD). Today, the BEM method is used extensively by wind turbine manufacturers to analyze the aerodynamic performance of a wind turbine. Although it is computationally fast and is easily implemented, it is acceptable only for a certain range of flow conditions.[1] A number of empirical and semi-empirical correction factors have been added to the BEM method in order to increase its application range, such as yaw misalignment, dynamic inflow, finite number of blades and blade cone angle[2] but they are not relevant to all operating conditions and are often incorrect at high tip speed ratios where wake distortion is significant.[3] Moreover, because of the axisymmetric inflow assumption for the BEM method, it is no longer valid to predict the aerodynamic loads (because of non-uniform blade load) on rotor blades when the wind turbine operates under the yaw condition. Therefore, it has been modified by different engineering approaches such as disk averaged induced velocity, advancing and retreating blade effect, skewed wake geometry with trailing vortices and skewed wake geometry with root vorticity. These engineering approaches were originally based on the disk averaged velocity on an annular ring explained in Refs. 4 and 5, even though their application is limited for small yaw angles.[6]

Apart from the traditional BEM and the advanced CFD methods, the vortex method which is based on the potential, inviscid and irrotational flow can be used to predict the aerodynamic performance of wind turbines. It has been widely used for aerodynamic analysis of airfoils and aircrafts. Compared with the BEM method, the vortex method is able to provide more physical solutions for attached flow conditions with boundary layer corrections, and it is also valid over a wider range of turbine operating conditions. Although it is computationally more expensive than the BEM method, it is still feasible as an engineering method.

In the vortex methods, the trailing wake is modeled by either vortex particles or vortex filaments moving either freely, known as free wake,[7–11] or restrictedly by imposing the wake geometry known as prescribed wake.[12,13] The free wake model, which is the most computationally expensive vortex method, is able to predict the wake geometry and loads more accurately than the prescribed wake. In addition, contrary to the BEM method, the free wake model can be applied for both axisymmetric and asymmetric (e.g. yaw condition, wind shear and etc) upstream flow conditions especially for yawed flow where the effects of the skewed wake is automatically taken into account. Hence, because of the complex structure of the trailing wake due to the yaw misalignment, the free wake model may be an appropriate method which provides more details of the wake aerodynamics.

As mentioned in the first paragraph, the yaw misalignment makes a time varying and 3D aerodynamic environment for a horizontal axis wind turbine (HAWT) because of its periodic attribute. As an example, one of the most important features of a wind turbine operating under the yaw condition is the advancing and retreating effect due to the blade rotation. The reason for this effect is the lateral component of the incoming velocity which makes the inflow at the rotor blade dependent on the blade azimuthal position. As a consequence, a temporal variation of the circulation around the blade section during the blade rotation generates an additional vorticity even if the upstream flow is steady and uniform. This extra vortex shedding along with the trailing vortices strongly influences the induced velocity field which in turn affects the wake geometry.[14] Moreover, the advancing and retreating effect due to the yawed flow means that the blades are subjected to different angle of attacks despite the steady and uniform inflow. This makes an extra moment which is called yaw moment due to the imbalance of the forces and moments acting on the hub.[15]

Because of the asymmetrical structure of the yaw misalignment, it creates unsteady aerodynamic sources. In the BEM method, an engineering approach called Dynamic Inflow model is introduced to take the unsteady aerodynamic features of the wind turbine into account. In other words, the aim of the dynamic inflow model is to predict the effect of the time varying vortex wake structures of the incoming flow at the rotor plane. Although the recently developed dynamic inflow models[5] take axisymmetric conditions into account such as transient blade pitching, however their applications are limited for yawed flow as an asymmetric condition. On the other hand, the VLFW model is able to predict a detailed time-accurate velocity field over the rotor plane for a broad range of wind turbine operating conditions without any approximation.[6]

The time-marching vortex lattice free wake is used in the present work to study the effect of yaw misalignment on the wake aerodynamics of a horizontal axis wind turbine. The results are compared with the MEXICO project experimental data.[16] The MEXICO wind turbine measurements were carried out in 2006 in the Large Scale Low Speed Facility (LLF) of the German Dutch Wind Tunnel (DNW).

II. Model

II.A. Assumptions

In this study, the upstream flow is set to be uniform, both in time and space while it is not perpendicular to the rotor plane (it deviates from the rotating axis). However our code can handle both uniform or non-uniform flow (varying both in time and space). The blades are assumed to be rigid. Therefore, the elastic effects of the blades are neglected.

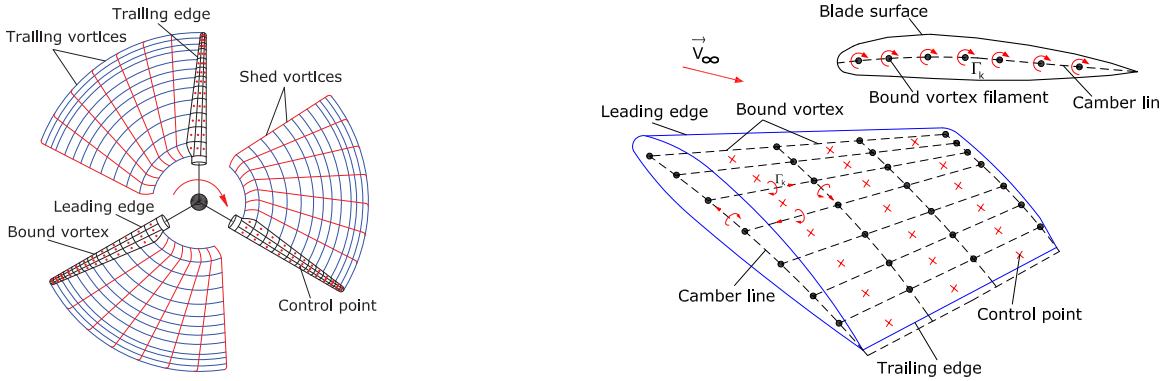

Figure 1. Left: Schematic of vortex lattice free wake, Right: Lifting surface and vortex panels construction

II.B. Vortex Lattice Free Wake (VLFW)

The vortex lattice method is based on the thin lifting surface theory of vortex ring elements,[17] in which the blade surface is replaced by vortex panels that are constructed based on the airfoil camber line of each blade section (see figure 1). To take the blade surface curvature into account, the lifting surface is divided into a number of panels, both in the chordwise and spanwise directions, where each panel contains a vortex ring with strength Γ_{ij} in which i and j indicate panel indices in the chordwise and spanwise directions, respectively. The strength of each blade bound vortex ring element, $\Gamma_{i,j}$, is assumed to be constant, and the positive circulation is defined on the basis of the right-hand rotation rule.

In the vortex lattice free wake model, a finite number of vortex wake elements move freely based on the local velocity field, and contrary to the prescribed wake model, allowing wake expansion as well. Each vortex filament contains two points; one at the head and another at the tail. They are known as Lagrangian markers, where the induced velocity components are calculated using the Biot-Savart law; their movements give rise to the wake deformation. The vortex flow theory assumes that the trailing and shed wake vortices extend to infinity. Nevertheless, according to Ref. 18, since the effect of the induced velocity field by the far wake is small on the rotor blade, the wake extends only four diameters downstream of the wind turbine rotor plane for the load calculation.

In order to fulfill the 2D Kutta condition (which can be expressed as $\gamma_{T.E.} = 0$ in terms of the strength of the vortex sheet where the $T.E.$ subscripts denotes the trailing edge) the leading segment of a vortex ring is located at $1/4$ of the panel length. The control point of each panel is located at $3/4$ of the panel length meaning that the control point is placed at the center of the panel's vortex ring.

The wake elements which induce a velocity field around the blade are modeled as vortex ring elements, and they are trailed and shed based on a time-marching method. To satisfy the 3D trailing edge condition for each spanwise section, the strength of the trailing vortex wake rings must be equal to the last vortex ring row in the chordwise direction ($\Gamma_{T.E.} = \Gamma_{Wake}$). This mechanism allows that the blade bound vorticity is transformed into free wake vortices.

The flow tangency condition at each blade's control point must be specified to find the blade bound vortices strength ($\Gamma_{i,j}$) at each time step. The velocity components at each blade's control point include the free stream ($\vec{V}_\infty$), rotational ($\Omega\vec{r}$), blade vortex rings self-induced ($\vec{V}_{ind,bound}$) and wake induced ($\vec{V}_{ind,wake}$) velocities.

The blade is assumed to be rigid, hence the blade self-induced components, called influence coefficients, are constant, and they are computed only once. However, if the blade would be modeled as a flexible blade, they would need to be calculated at each time step.

The governing equation for the wake geometry is

$$\frac{d\vec{r}}{dt} = \vec{V}_{tot}(\vec{r},t) \qquad \vec{r}(t=0) = \vec{r}_0 \tag{1}$$

where $\vec{r}$, $\vec{V}_{tot}$ and t denote the position vector of a Lagrangian marker, the total velocity field and time. The total velocity field, expressed in the rotating reference frame i.e. $\vec{V}_{rot} = 0$, can be written as

$$\vec{V}_{tot} = \vec{V}_{\infty} + \vec{V}_{ind,blade} + \vec{V}_{ind,wake} \tag{2}$$

Different numerical schemes may be used for Eq.(1) such as the explicit Euler method, the implicit method, Adams-Bashforth method and the Predictor-Corrector method. The numerical integration scheme must be considered in terms of the accuracy, stability and computational efficiency. Here, the first-order Euler explicit method is used as

$$\vec{r}_{t+1} = \vec{r}_t + \vec{V}_{tot}\,(\vec{r}_t)\,\Delta t \tag{3}$$

where $\vec{V}_{tot}$ is taken at the old time step.

III. Results

The three-bladed MEXICO wind turbine[16] is used in the simulation. The operating conditions at which the measurement were made[16] are: $\theta = 30^{\circ}$, $V_{tunnel} = 14.99\ m/s$, $\Omega = 44.45\ rad/s$, $\rho = 1.237\ kg/m^3$ where θ, V, Ω and ρ denote the yaw angle, free stream velocity, rotational velocity and the air density, respectively. Moreover, the rotor diameter, the blade length and the blade pitch angle are 4.5 m, 2.04 m and -2.3 degrees, respectively[16] and the positive yaw angle is defined as clockwise with respect to the radial (y) axis. In the vortex method simulations made

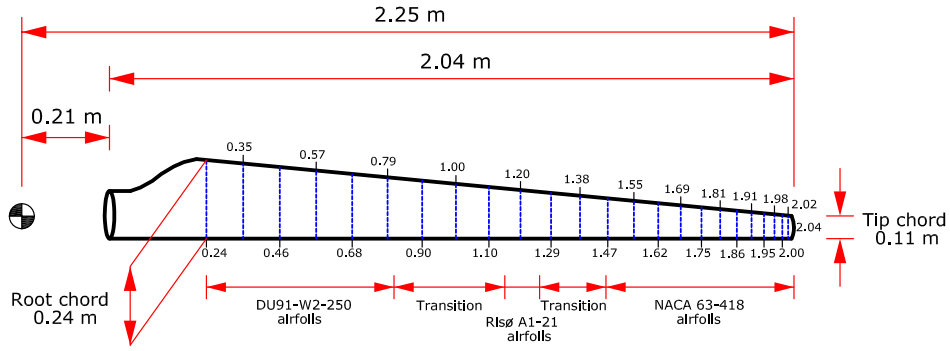

Figure 2. Schematic of radial distribution of blade elements

with VLFW in-house code, the blade is discretized with 24 spanwise sections (see figure 2) and 10 equally spaced chordwise sections. Because of the large circulation gradients $(d\Gamma/dr)$ near the tip of the rotor blade, the cosine rule for the blade radial segmentation[2] is used where the blade elements are distributed at equi-angle increments in the spanwise direction resulting in a fine tip resolution. 10 degrees in the azimuthal direction is employed for the wake segmentation.[18] In order to avoid the effect of the start-up vortex on the velocity field around the rotor blades, the wake length is truncated after 16 full rotor revolution (7.5 rotor diameters). It is indeed larger than the wake truncation length which is based on a grid-sensitivity study according to Ref. 18. It is assumed that the wake vortex filament core radius is constant and is equal to 0.1 m. Moreover, the free stream is assumed to be uniform and steady deviated $+30$ degrees with respect to the rotor axis as the measurements.

III.A. Radial and axial streaklines

The vortex core size is one of the most important parameters in the free vortex wake models which affects the vortex roll-up and wake development. In this subsection, the effect of the vortex core radius on the radial and axial streaklines is studied. Three different vortex core radii are employed i.e. 0.05 m, 0.1 m and 0.2 m, respectively. For all cases, the operating condition is set to be $V_{\infty} = 14.99$ m/s and $\Omega = 44.45$ rad/s while it is assumed that upstream flow is steady, uniform and perpendicular to the rotor plane (non-yawed condition).

Figures 4 and 5 show the streaklines of the trailing wake vortices of blade 1 at zero degrees of azimuth ($\Psi = 0^{\circ}$) for non-yawed condition extracted based on the last 6 revolutions (3 rotor diameters wake length). The radial streaklines are calculated on the basis of the radial positions ($r = \sqrt{(x^2 + y^2)}$) of the free wake vortices originating at the trailing edges of blade 1 in the xy plane (rotor plane) while the axial streaklines display the axial positions of the free wake vortices in the z direction (model coordinate system).

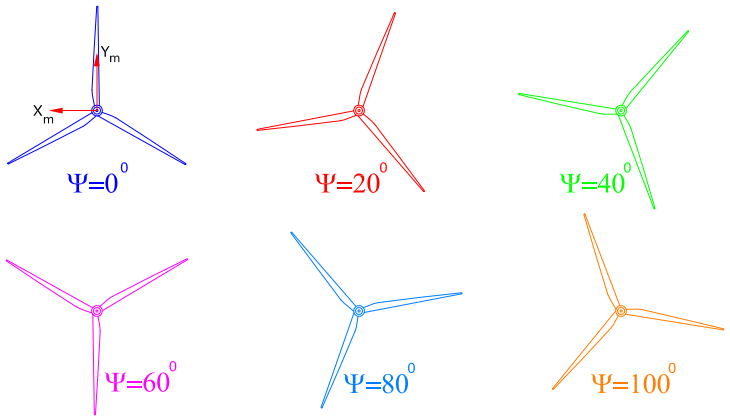

Figure 3. Position of rotor blades at different azimuthal angles, blade 1 at 0 degrees is pointing vertically upward, the model coordinate system is the inertial coordinate system with origin at hub

As seen in figures 4 and 5, choosing a large vortex core size delays the vortex roll-up (see figure 4 for $t < 0.1$ s). On the other hand, a small vortex core size does not significantly affect the tip vortex roll-up, but it makes the trailing wake vortices to deflect earlier which increases the wake instability (see figures 4 and 5 for $t > 0.6$ s). Therefore, as described in the Model section, choosing $r_{core} = 0.1$ m is found to be an appropriate value for the VLFW simulation. Hence, it is employed for the VLFW simulation yawed condition as well.

Figures 4 and 6 show that the vortex roll-up occurs in the vicinity of the tip and root of the blades. Although both non-yawed and yawed flows predict almost the same vortex roll-up positions, the wake is not expanded symmetrically for the yaw condition which is in contrast to the non-yawed flow. Beside the fact that yaw misalignment makes the trailing wake to evolve periodically (see figure 6), comparing figures 4, 5 and 6 reveal that in the yawed flow, because of the in-plane velocity component (V_x), the trailing vortex wake becomes more unstable during its evolution.

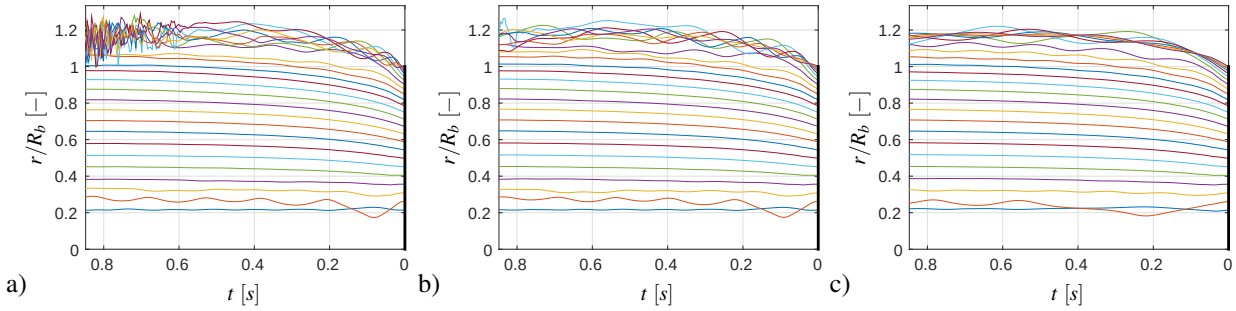

Figure 4. Radial streaklines of trailing vortices for different vortex core size at 0° yaw angle, *a*) $r_{core} = 0.05$ **m,** *b*) $r_{core} = 0.1$ **m,** *c*) $r_{core} = 0.2$ **m**

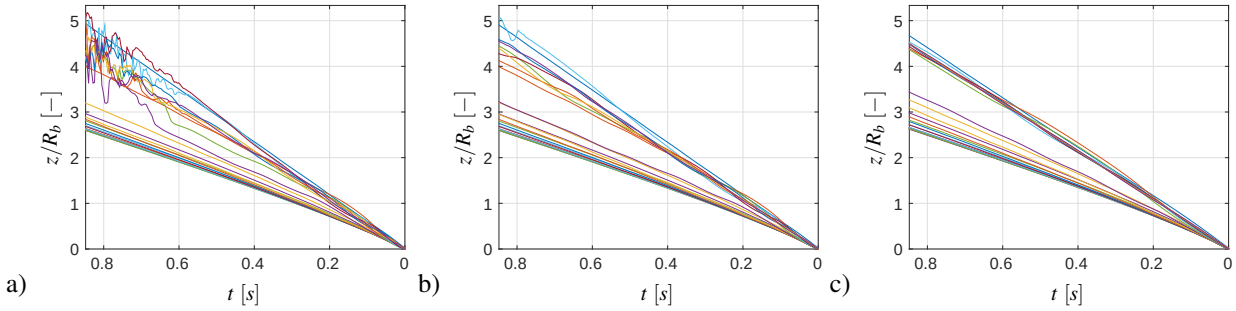

Figure 5. Axial streaklines of trailing vortices for different vortex core size at 0° yaw angle, *a*) $r_{core} = 0.05$ **m,** *b*) $r_{core} = 0.1$ **m,** *c*) $r_{core} = 0.2$ **m**

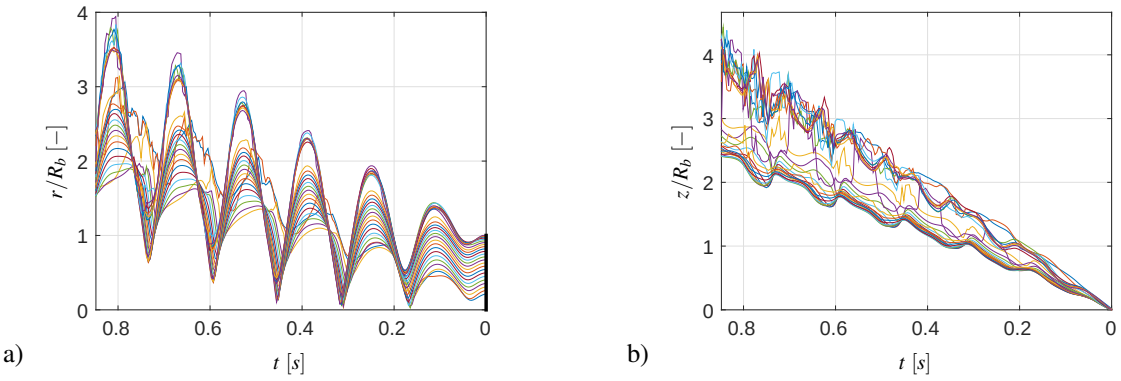

Figure 6. Streaklines of trailing vortices at 30° yaw angle and constant vortex core radius $r_{core} = 0.1$ m, *a*) Radial, *b*) Axial

III.B. Radial traverses

For the radial traverses, the velocity field is measured both upstream and downstream of the rotor at different blade positions (see figure 3). The horizontal plane which approximately covers the region from one tip to the other (see figure 7), extends from $z = -0.15\ m$, upstream of the rotor, to $z = +0.15\ m$, downstream of the rotor ($z = 0$ is in the rotor plane). In addition, the horizontal plane extends from $x = -3.0\ m$ to $x = +3.0\ m$ (**IJ** and **KL** lines) where $x = 0$ is in the rotor centre.[16] For the radial traverses measurements, all geometry coordinates (x, y, z) are defined on the basis of the model (inertial) coordinate system whereas the velocity components (u, v, w) are measured with respect to the tunnel coordinate system.

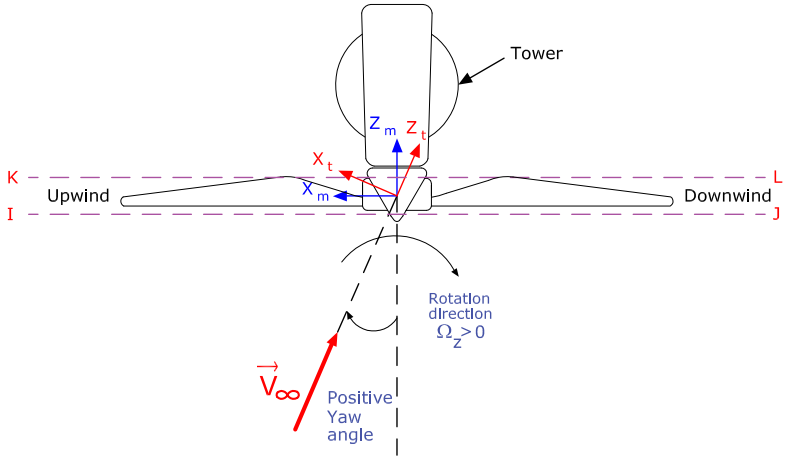

Figure 7. Schematic of radial traverses, m and t subscripts denote model and tunnel coordinates, respectively

Figures 10 to 21 display the velocity components along two radial traverses. The agreement between the simulations and the measurement is good. The calculated velocity components by the simulation include the free stream velocity, induced velocity by the trailing wake and induced velocity by the rotor blades . The results confirm that the induction effect of the rotor blades ($\vec{V}_{ind,blade}$) on the radial traverses is small both upstream and downstream except for radial component v (see figures 8 and 9) depending on the rotor blades position at different azimuthal angles. The abrupt change downstream of the rotor for both axial and tangential velocities occurs because of the presence of the tip vortex which accordingly influences the flow behind the rotor. As seen in sub-figure (a) in figures 10 to 21, there are two considerable extrema both downstream and upstream of the rotor in the vicinity of the blade tip. The simulation shows the same tangential velocity magnitudes and the same positions along the **IJ** line (upstream of the rotor) as the measurement does. Although the simulation predicts the the same extremum positions around $x = \pm 2.5$m (blade radius) along the **KL** line (downstream of the rotor), it underestimates the magnitude of one of the extrema depending on the rotor azimuthal angle (Ψ). Furthermore, the positive tangential velocity at the positive x positions and the negative tangential velocity at the negative x positions along the **IJ** line reveal that the trailing wake expands laterally. However, because of the different magnitude of the tangential velocity at the positive and negative x direction, the wake does

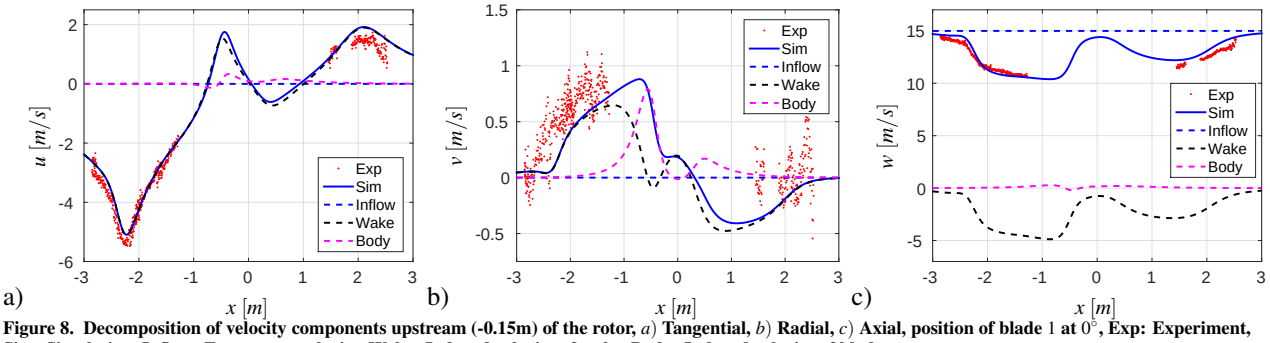

Figure 8. Decomposition of velocity components upstream (-0.15m) of the rotor, *a*) Tangential, *b*) Radial, *c*) Axial, position of blade 1 at 0°, Exp: Experiment, Sim: Simulation, Inflow: Freestream velocity, Wake: Induced velocity of wake, Body: Induced velocity of blade

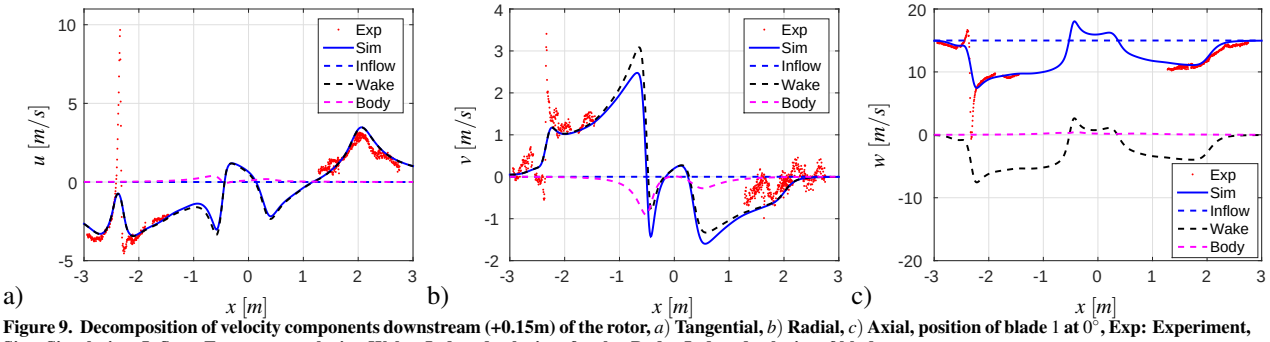

Figure 9. Decomposition of velocity components downstream (+0.15m) of the rotor, *a*) Tangential, *b*) Radial, *c*) Axial, position of blade 1 at 0°, Exp: Experiment, Sim: Simulation, Inflow: Freestream velocity, Wake: Induced velocity of wake, Body: Induced velocity of blade

not expand symmetrically showing much larger wake expansion downwind of the rotor plane than upwind of the rotor plane (see figure 7).

Sub-figure (b) in figures 10 to 21 displays the radial velocity component (v). Despite the good agreement for tangential and axial velocities, there is poor agreement between the simulation and experimental data. However, it should be noted that the apparent poor agreement is mainly due to the small magnitude of the radial velocity. The radial velocity induced by the rotor blade is not negligible, which is in contrast to the tangential and axial velocities. This means that, in addition to the induced velocity by trailing wake vortices, the rotor blade makes the wake to expand radially.

The axial velocity component (w) is shown in sub-figure (c) of figures 10 to 21. A well quantitative agreement between the simulation and experimental data can be observed. The presence of the tip vortex makes a significant change in the axial velocity in the vicinity of the blade tip. This is verified by both simulation and measurements even though the simulation predicts smaller peak magnitudes. The radial tip vortex position downstream of the rotor blades describes the wake expansion. For the non-yawed condition, as shown in Ref. 19, the measurement gives a slightly larger radial position than the simulation, but for the yawed flow, it is seen that both simulation and measurements give almost the same tip vortex position, equal to the blade tip radius. This means that, close to the rotor plane, the wake expansion rate for yawed condition is smaller than for non-yawed condition[20] even if the wake does not expand symmetrically.

III.C. Axial traverses

For the axial traverses, the velocity field is measured at four different spanwise sections of the blade (see figure 22). The two positive locations (**AB** and **CD** lines) are at $x = +1.37697\ m$ and $x = +1.84697\ m$ while the negative ones (**EF** and **GH** lines) are at $x = -1.37697\ m$ and $x = -1.84697\ m$. For the positive midboard (**CD**) and outboard (**AB**) positions, blade 1 is located at zero degrees of azimuthal angle whereas for the negative midboard (**EF**) and outboard (**GH**) positions, blade 1 is located at 60 degrees of azimuthal angle (see figure 3). The horizontal plane, parallel to the rotor axis (see figure 22), extends from $z = -4.5\ m$, upstream of the rotor, to $z = +5.9\ m$, downstream of the rotor where $z = 0$ is at the rotor plane. It is noted that for the axial traverses measurements, all variables (x, y, z, u, v, w) are defined on the basis of the tunnel coordinate system.

Figures 23 to 26 display the velocity components for the axial traverses. There is a quite good agreement be-

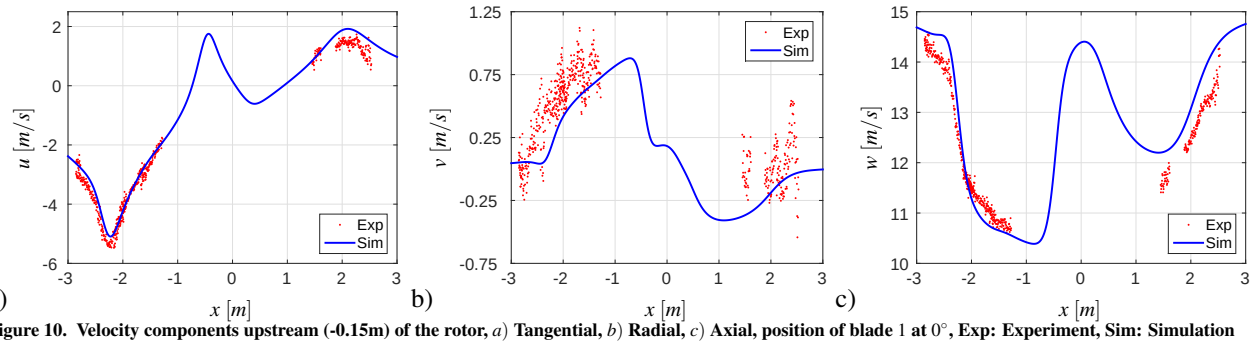

Figure 10. Velocity components upstream (-0.15m) of the rotor, *a*) Tangential, *b*) Radial, *c*) Axial, position of blade 1 at 0°, Exp: Experiment, Sim: Simulation

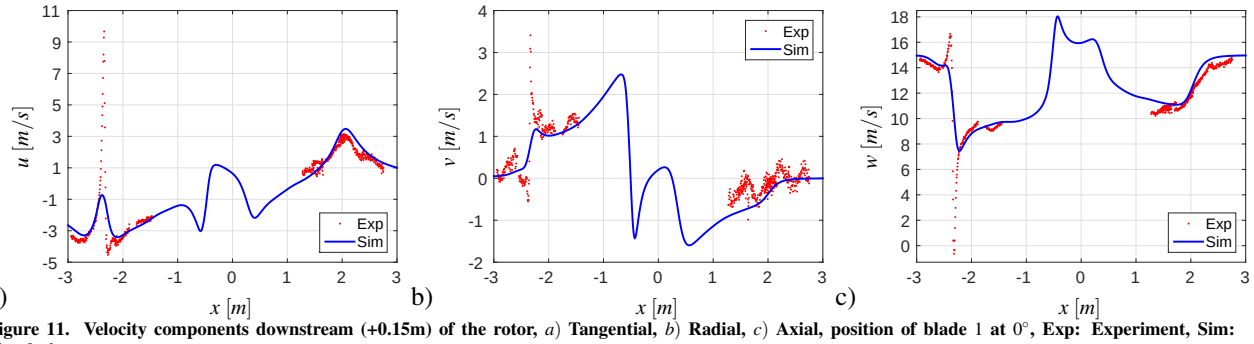

Figure 11. Velocity components downstream (+0.15m) of the rotor, *a*) Tangential, *b*) Radial, *c*) Axial, position of blade 1 at 0°, Exp: Experiment, Sim: Simulation

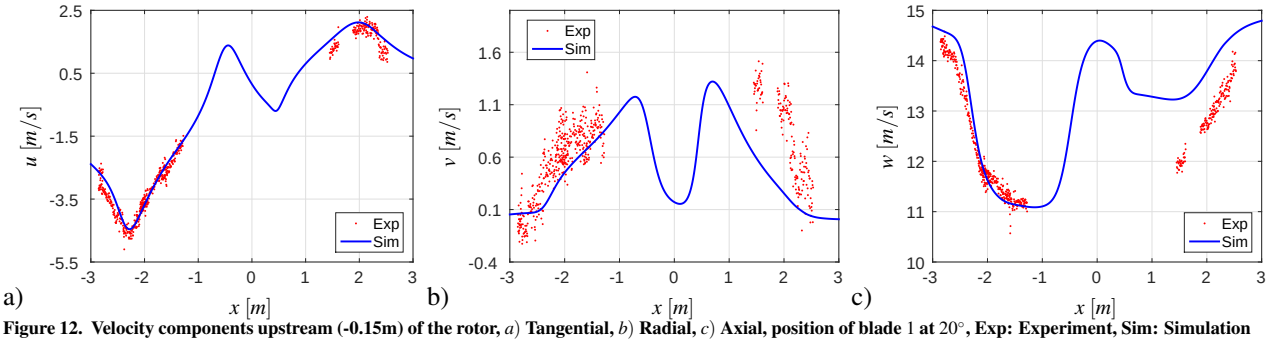

Figure 12. Velocity components upstream (-0.15m) of the rotor, *a*) Tangential, *b*) Radial, *c*) Axial, position of blade 1 at 20°, Exp: Experiment, Sim: Simulation

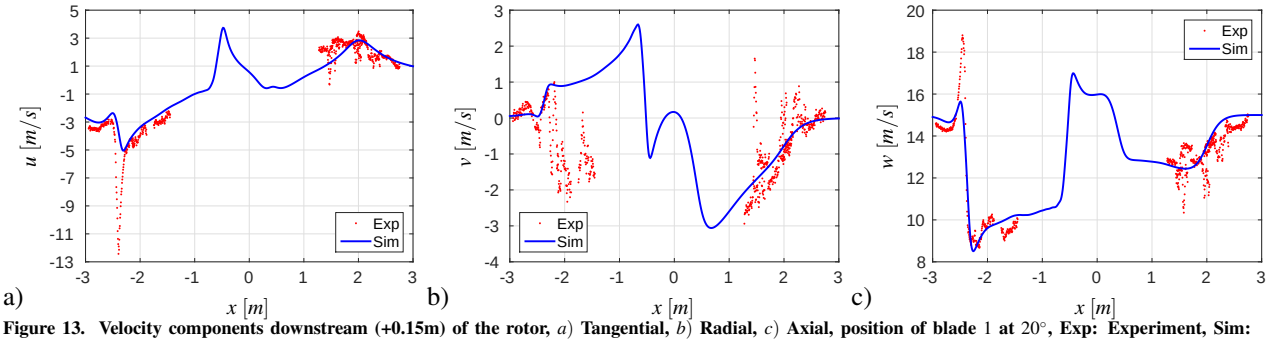

Figure 13. Velocity components downstream (+0.15m) of the rotor, *a*) Tangential, *b*) Radial, *c*) Axial, position of blade 1 at 20°, Exp: Experiment, Sim: Simulation

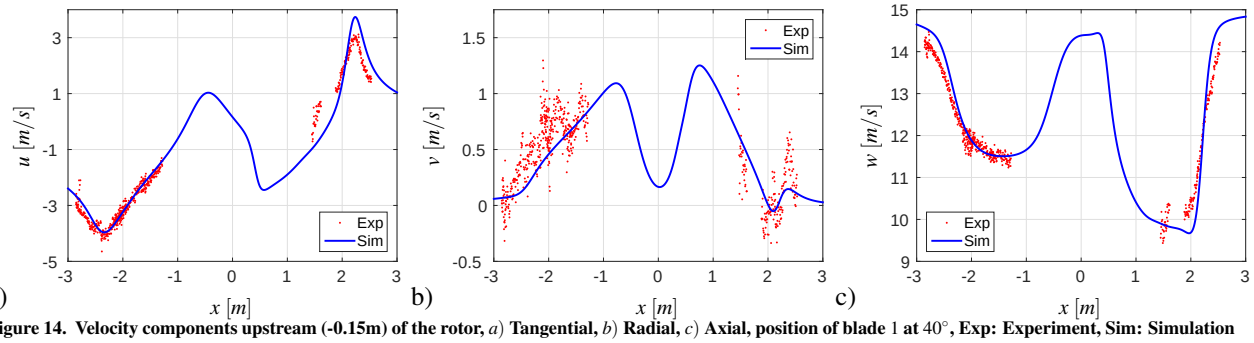

Figure 14. Velocity components upstream (-0.15m) of the rotor, *a*) Tangential, *b*) Radial, *c*) Axial, position of blade 1 at 40°, Exp: Experiment, Sim: Simulation

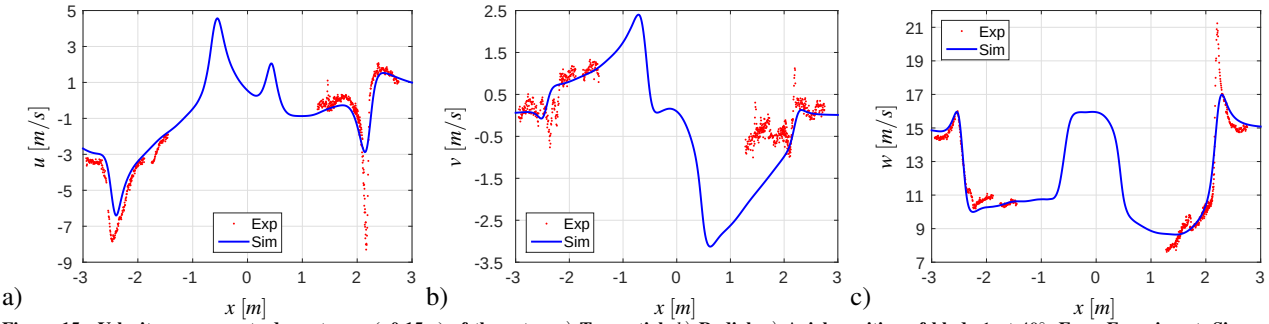

Figure 15. Velocity components downstream (+0.15m) of the rotor, *a*) Tangential, *b*) Radial, *c*) Axial, position of blade 1 at 40°, Exp: Experiment, Sim: Simulation

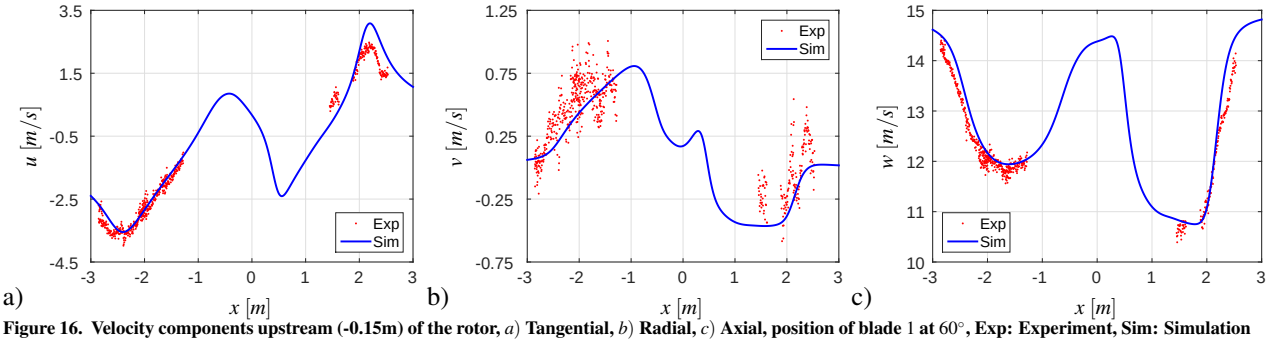

Figure 16. Velocity components upstream (-0.15m) of the rotor, *a*) Tangential, *b*) Radial, *c*) Axial, position of blade 1 at 60°, Exp: Experiment, Sim: Simulation

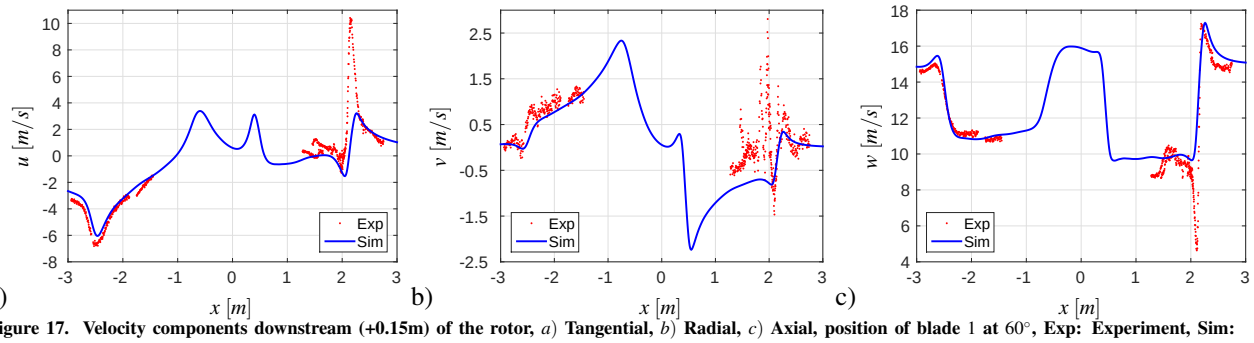

Figure 17. Velocity components downstream (+0.15m) of the rotor, *a*) Tangential, *b*) Radial, *c*) Axial, position of blade 1 at 60°, Exp: Experiment, Sim: Simulation

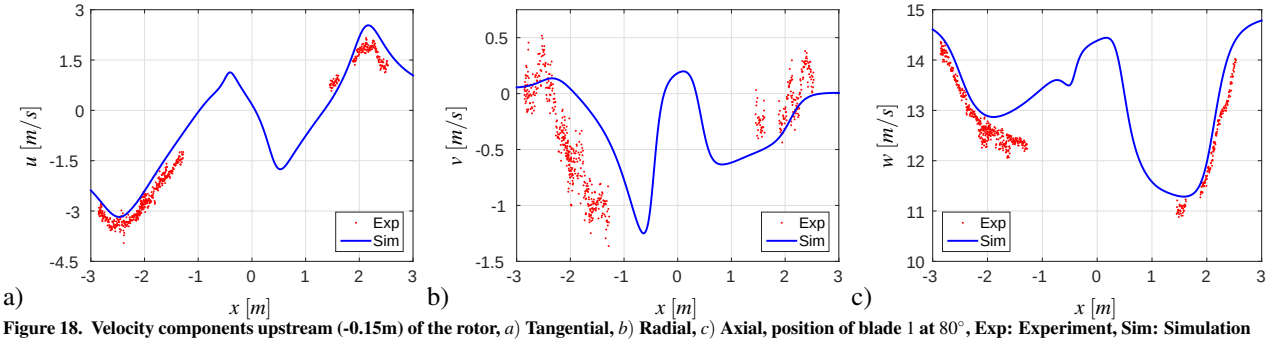

Figure 18. Velocity components upstream (-0.15m) of the rotor, *a*) Tangential, *b*) Radial, *c*) Axial, position of blade 1 at 80°, Exp: Experiment, Sim: Simulation

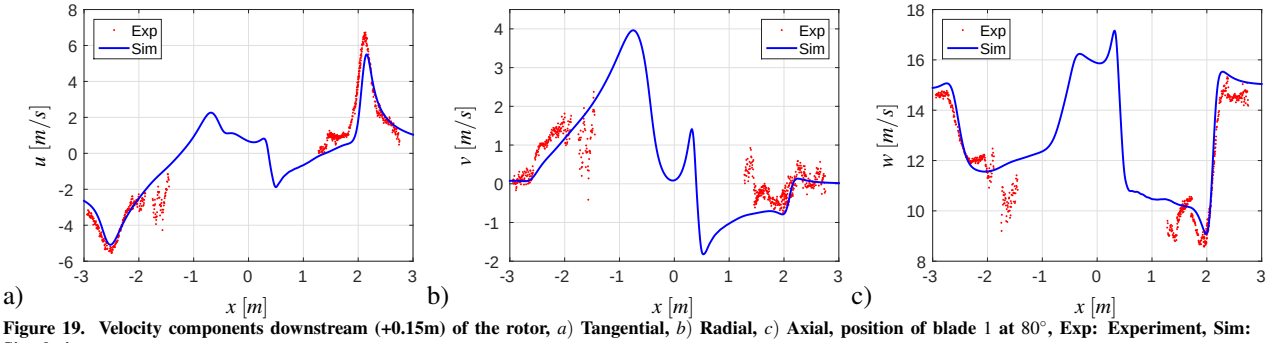

Figure 19. Velocity components downstream (+0.15m) of the rotor, *a*) Tangential, *b*) Radial, *c*) Axial, position of blade 1 at 80°, Exp: Experiment, Sim: Simulation

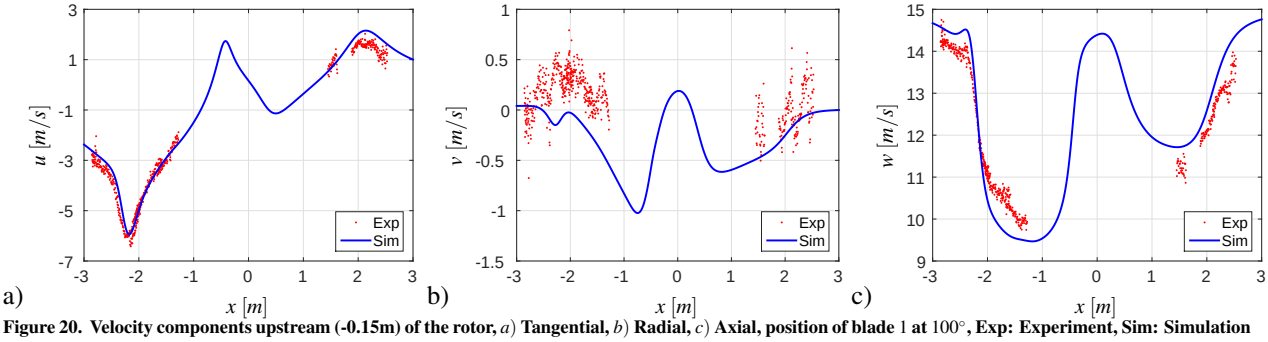

Figure 20. Velocity components upstream (-0.15m) of the rotor, *a*) Tangential, *b*) Radial, *c*) Axial, position of blade 1 at 100°, Exp: Experiment, Sim: Simulation

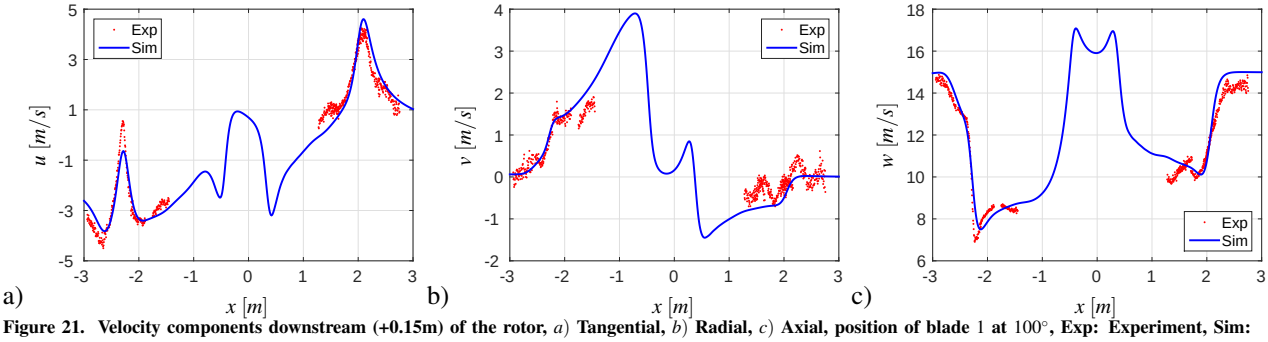

Figure 21. Velocity components downstream (+0.15m) of the rotor, *a*) Tangential, *b*) Radial, *c*) Axial, position of blade 1 at 100°, Exp: Experiment, Sim: Simulation

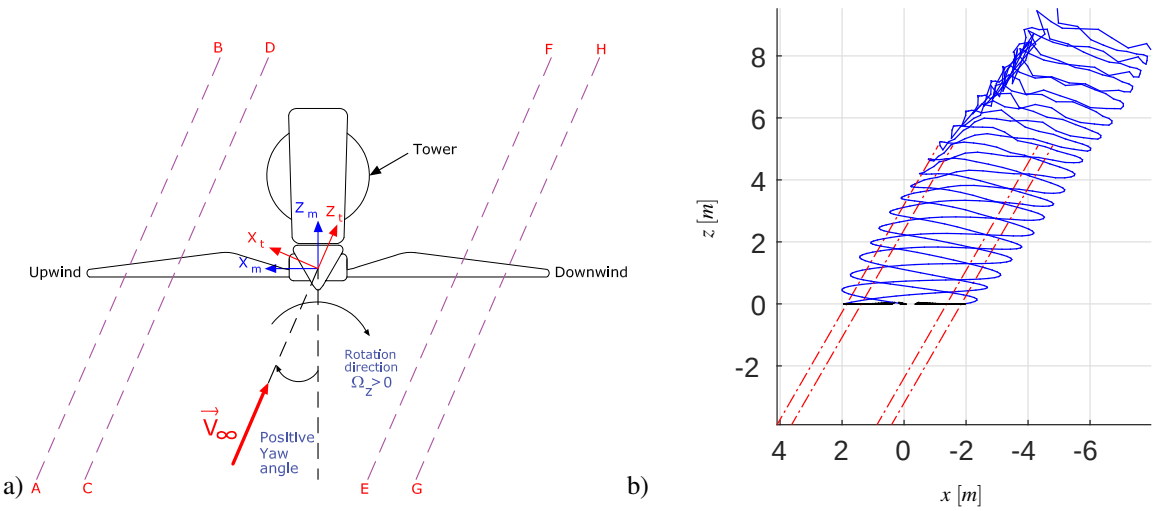

Figure 22. a) Schematic of axial traverses, m and t subscripts denote model and tunnel coordinates, respectively b) Blades Tip vortices and axial traverses

tween the simulation and measurement for the negative lines (**EF** and **GH**) whereas considerable discrepancies for the positive lines (**AB** and **CD**) are observed. The major reason for this difference, which has been also mentioned in Refs. 10, 21 and 22, is that in the VLFW simulation, the turbine's nacelle is not modeled. Nonetheless, the effect of the nacelle is limited only for a certain length of the **AB** and **CD** lines which roughly extends from 1.0 m to 4.0 m.

Sub-figure (a) in figures 23 and 24 shows the tangential velocity (u) along the negative axial traverses (**EF** and **GH**). It is observed that the tangential velocity is negative along these lines where it decreases gradually until $z = 1$ m, and then it increases successively. The behavior of the tangential velocity downstream of the rotor plane (negative values and positive slope) implies that the expansion rate of the wake in the negative x direction decreases when moving downstream along the axial traverses as confirmed by figure 22 (b). Moreover, as explained in the axial and radial streaklines subsection, the fluctuating tangential velocity downstream of the rotor plane may be enhanced due to the fact that the yaw misalignment makes the trailing wake to evolve periodically.

Sub-figure (a) in figures 25 and 26 presents the tangential velocity along the positive axial traverses (**AB** and **CD**). As mentioned earlier in this subsection, the omission of the nacelle model in the VLFW simulation makes a big difference between the simulation and measurement downstream of the rotor. However, this discrepancy is smaller for the tangential velocity. Furthermore, the tangential velocity along the positive transect show that the wake is deflected more in the negative x direction, compared to the negative axial transect. As observed in figure 22 (b), the trailing wake vortices are remarkably disturbed upwind side of the rotor plane (see figure 22). This makes the tangential velocity oscillates a lot along the positive axial traverses especially for the positive outboard (**AB**).

There is a qualitative agreement between the simulation and measurement data for the radial velocity (v) as presented in sub-figure (b) of figures 23 to 26. The positive magnitude of the radial velocity after the rotor center ($z = 0$ m) verifies that not only does the wake expand tangentially, but also radially.

The axial velocity (w) for different axial traverses are presented in sub-figure (c) of figures 23 to 26. For the negative midboard and outboard axial transects the axial velocity decreases gradually and it approaches a constant value slightly downstream of the rotor plane (half a rotor diameter). The large difference between the simulated and measured axial velocities for the positive traverses between 1.0 m and 4.0 m were described earlier (nacelle effect). Nevertheless, oscillations of the axial velocity slightly upstream and downstream the rotor center ($z = 0$ m) may be explained by the proximity of the positive outboard transect to the highly distorted trailing wake upwind side of the rotor plane. In addition, the axial velocity along the positive midboard (**AB**) recovers fast and gets even larger than the undisturbed free stream ($\vec{V}_\infty = 14.99$ m/s). This may be explained by the smaller expansion (weak induced velocity field) at the upwind side of the rotor plane making the positive outboard transect to be out of the wake to some extent (see figure 22 (b)).

IV. Conclusion

A time-marching vortex lattice free wake (VLFW) model has been developed to study the wake aerodynamics of a horizontal axis wind turbine. To validate, the model has been used to simulate the flow field around the MEXICO

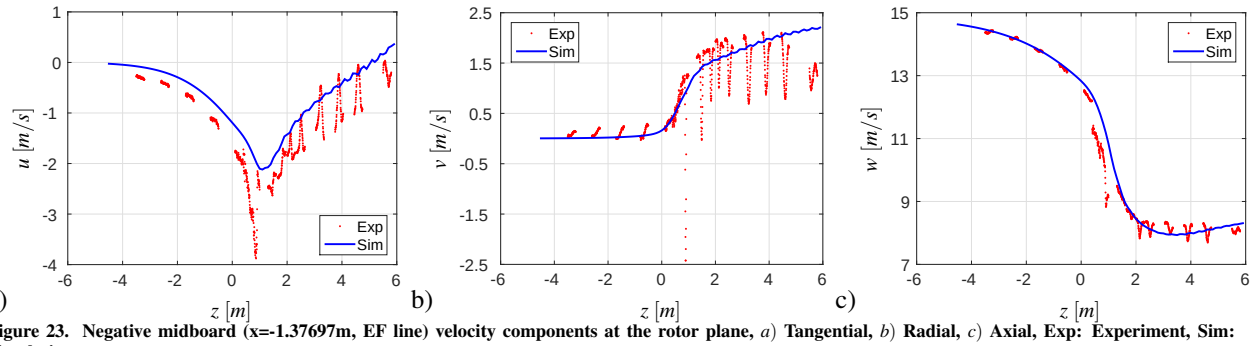

Figure 23. Negative midboard (x=-1.37697m, EF line) velocity components at the rotor plane, *a*) Tangential, *b*) Radial, *c*) Axial, Exp: Experiment, Sim: Simulation

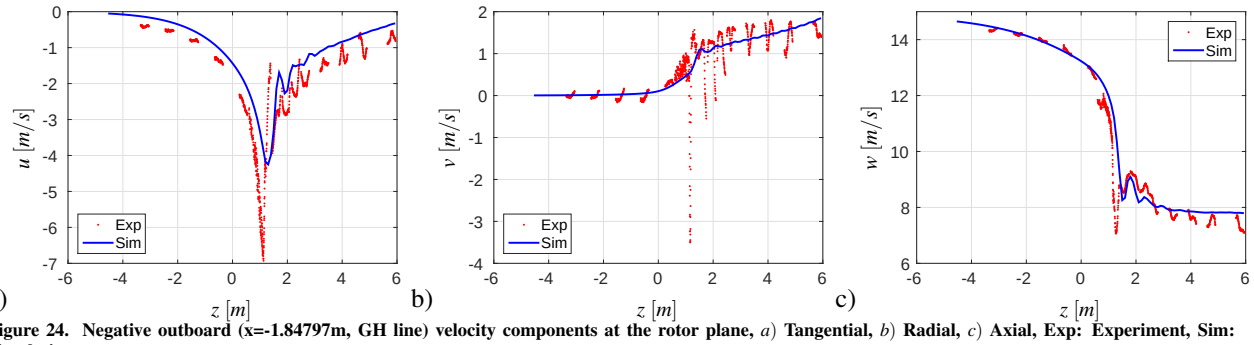

Figure 24. Negative outboard (x=-1.84797m, GH line) velocity components at the rotor plane, *a*) Tangential, *b*) Radial, *c*) Axial, Exp: Experiment, Sim: Simulation

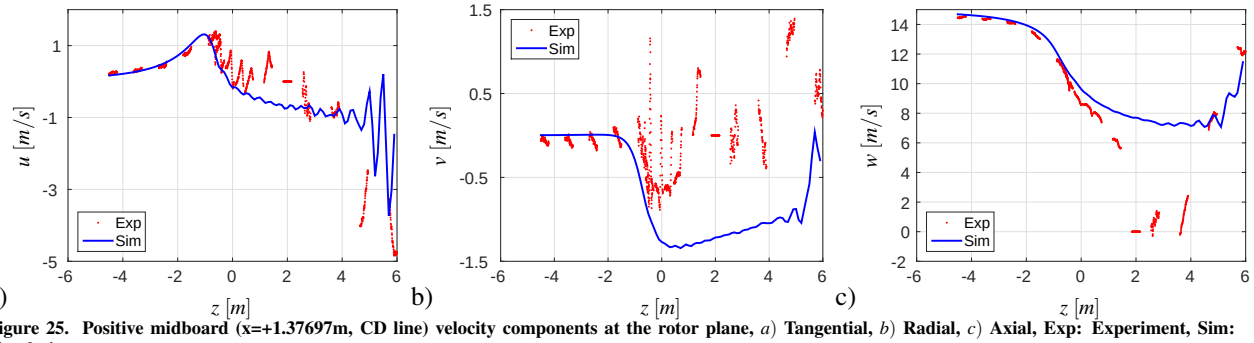

Figure 25. Positive midboard (x=+1.37697m, CD line) velocity components at the rotor plane, *a*) Tangential, *b*) Radial, *c*) Axial, Exp: Experiment, Sim: Simulation

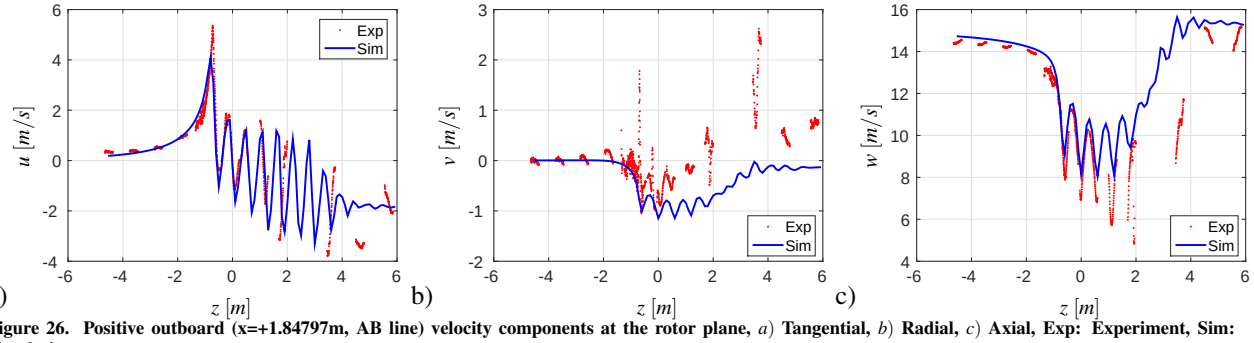

Figure 26. Positive outboard (x=+1.84797m, AB line) velocity components at the rotor plane, *a*) Tangential, *b*) Radial, *c*) Axial, Exp: Experiment, Sim: Simulation

turbine under yaw condition. The operating conditions, at which the measurement were made, are $\vec{V}_\infty = 14.99$ m/s, $\Omega = 44.45$ rad/s. The results of the VLFW simulation have been compared with the MEXICO experimental data where the upstream flow is steady, uniform with $+30$ degrees of yaw misalignment.

There is a good agreement between the simulation and experiments for the velocity field along the radial and axial traverses, both upstream and downstream of the rotor blades. Unlike the tangential and axial velocities, there is a rather poor agreement between the simulation and measurement for the radial velocity (v) showing that the rotational effects on the wake aerodynamics of the wind turbine are not well captured by vortex method. Moreover, the nacelle's wake on the computed velocity components along the positive axial traverses makes a significant discrepancies between the simulation and experimental results which shows that it is important to include the nacelle in the study of wind turbine wake aerodynamics.

Apart from the in-plane (tangential) velocity component of the yawed flow, employing a small vortex core size makes the trailing vortex wake becomes unstable early. Moreover, the wake evolution in time is asymmetrical under yaw condition which is in contrast to the non-yawed flow. Therefore, the trailing and shed wake vortices are expanded unequally resulting in a strong expansion downwind of the rotor and a weak expansion upwind of the rotor.

Acknowledgments

The data used have been supplied by the consortium which carried out the EU FP5 project MEXICO: 'Model rotor EXperiments In COntrolled conditions'.

The Swedish Wind Power Technology Centre (SWPTC) is a research centre for design of wind turbines. The purpose of the Centre is to support Swedish industry with knowledge of design techniques as well as maintenance in the field of wind power. The research in the centre is carried out in six theme groups that represent design and operation of wind turbines; Power and Control Systems, Turbine and Wind loads, Mechanical Power Transmission and System Optimisation, Structure and Foundation, Maintenance and Reliability as well as Cold Climate. This project is part of Theme group 2.

SWPTCs work is funded by the Swedish Energy Agency, by three academic and thirteen industrial partners. The Region Västra Götaland also contributes to the Centre through several collaboration projects.

References

[1]Hansen, M. O., *Aerodynamics Of Wind Turbines*, 2nd edition, EarthScan, 2008.

[2]van Garrel, A., *Development Of A Wind Turbine Aerodynamics Simulation Module*, ECN report, ECN-C–03-079, August 2003.

[3]Vermeer, L., Sørensen, J., and Crespo, A., "Wind Turbine Wake Aerodynamics," *Progress in Aerospace Sciences*, Vol. 39, 2003, pp. 467–510.

[4]Glauert, H., *The Analysis of Experimental Results in the Windmill Brake and Vortex Ring States of an Airscrew*, RCR R&M No. 1026, 1926.

[5]Snel, H. and Schepers, J., *Joint Investigation of Dynamic Inflow Effects and Implementation of an Engineering Method*, ECN-C-94-107, Petten, Energy Research Centre of the Netherlands April, 1995.

[6]Gupta, S. and Leishman, G., "Comparison of momentum and vortex methods for the aerodynamic analysis of wind turbines," *43rd AIAA Aerospace Sciences Meeting and Exhibit, Reno, Nevada*, 10-13 January 2005.

[7]Gupta, S., *Development of a Time-Accurate Viscous Lagrangian Vortex Wake Model for Wind Turbine Applications*, University of Maryland, Department of Aerospace Engineering, 2006.

[8]Pesmajoglou, S. and Graham, J., "Prediction Of Aerodynamic Forces On Horizontal Axis Wind Turbines In Free Yaw And Turbulence," *Journal of Wind Engineering and Industrial Aerodynamics*, Vol. 86, 2000, pp. 1–14.

[9]Voutsinas, S., "Vortex Methods In Aeronautics: How To Make Things Work," *International Journal of Computational Fluid Dynamics*, Vol. 20, 2006, pp. 3–18.

[10]Garcia, N. R., Sørensen, J., and Shen, W. Z., "Simulations of the Yawed MEXICO Rotor Using a Viscous-Inviscid Panel Method," *Journal of Physics: Conference Series*, Vol. 524, 2014.

[11]Garcia, N. R., Sørensen, J., and Shen, W. Z., "Development of a Three-Dimensional Viscous-Inviscid coupling Method for Wind Turbine Computations," *Proceedings of the 2013 International Conference on aerodynamics of Offshore Wind Energy Systems and wakes (ICOWES2013)*, 2013, pp. 569–81.

[12]Chattot, J., "Helicoidal Vortex Model For Wind Turbine Aeroelastic Simulation," *Computers and Structures*, Vol. 85, 2007, pp. 1072–1079.

[13]Chattot, J., "Optimization Of Wind Turbines Using Helicoidal Vortex Model," *Journal of Solar Energy Engineering*, Vol. 125, 2003, pp. 418–424.

[14]Voutsinas, S., Beleiss, M., and Rados, K., "Investigation of the Yawed Operation of Wind Turbines by means of a Vortex Particle Method," *AGARD Conference Proceedings*, Vol. 552, 1995, pp. 11.1–11.

[15]Hansen, A. C., "Yaw Dynamics of Horizontal Axis Wind Turbines," NREL Report No.: NRELFP-442-482, University of Utah Salt Lake City, Utah, April 1992.

[16]Schepers, J. and Boorsma, K., *Description of experimental setup MEXICO measurements*, Energy research Centre of the Netherlands, ECN-X–09-0XX, 2006.

[17]Katz, J. and Plotkin, A., *Low-Speed Aerodynamics*, Cambridge University Press, 2nd ed., 2001.

[18]Abedi, H., *Development of Vortex Filament Method for Aerodynamic Loads on Rotor Blades*, Licentiate thesis, Department of Applied Mechanics, Chalmers University of Technology, Göteborg, 2013.

[19]Abedi, H., Davidson, L., and Voutsinas, S., "Numerical studies of the upstream flow field around a horizontal axis wind turbine," *AIAA SciTech, 33rd Wind Energy Symposium, Kissimmee, Florida*, 5-9 January 2015.

[20]Grant, I., Parkin, P., and Wang, X., "Optical vortex tracking studies of a horizontal axis wind turbine in yaw using laser-sheet, flow visualisation," *Experiments in Fluids*, Vol. 23, 1997, pp. 513–519.

[21]Schepers, J., Pascal, L., and Snel, H., "First results from MexNext: analysis of detailed aerodynamic measurements on a 4.5 m diameter rotor placed in the large German Dutch Wind Tunnel DNW," Technical report ecn-m-10-045, ECN, June 2010.

[22]Sørensen, N. N., Bechmann, A., Réthoré, P., and Zahle, F., "Near wake Reynolds-averaged Navier-Stokes predictions of the wake behind the MEXICO rotor in axial and yawed flow conditions," *Wind Energy*, Vol. 17, 2014, pp. 75–86.